Journal of Materials Chemistry C

PAPER

View Article Online
View Journal | View Issue

Cite this: J. Mater. Chem. C, 2014, 2, 6376

The unusual electronic structure of ambipolar dicyanovinyl-substituted diketopyrrolopyrrole derivatives†

A. Riaño,[a] P. Mayorga Burrezo,[b] M. J. Mancheño,[a] A. Timalsina,[c] J. Smith,[c] A. Facchetti,[c] T. J. Marks,*[c] J. T. López Navarrete,*[b] J. L. Segura,*[a] J. Casado[b] and R. Ponce Ortiz*[b]

Received 8th April 2014
Accepted 30th May 2014

DOI: 10.1039/c4tc00714j

www.rsc.org/MaterialsC

We have synthesized two novel dicyanovinylene-substituted DPP–oligothiophene semiconductors, **DPP-4T-2DCV** and **2DPP-6T-2DCV**. In these materials, the combination of an extended oligothiophene conjugated skeleton with the strong electron-withdrawing DPP–dicyanovinylene groups results in semiconductors exhibiting ambipolar TFT response with reasonably balanced electron and hole mobilities of up to 0.16 $cm^2 V^{-1} s^{-1}$ and 0.02 $cm^2 V^{-1} s^{-1}$, respectively. Furthermore, no thermal annealing of the semiconductors is necessary to afford high mobility, making them ideal candidates for low cost fabrication of devices on inexpensive plastic foils. Analysis of the molecular and electronic structures by means of electronic and vibrational spectroscopy techniques, electrochemistry and DFT calculations highlights a unique electronic scenario in these semiconductors, where the external cyano groups are isolated from the π-conjugated core. The appearance of these unusual π-systems explains the similar electron mobilities recorded for both **DPP-4T-2DCV** and **2DPP-6T-2DCV**, despite their different skeletal dimensions. Furthermore, it also supports the appearance of moderately balanced hole and electron mobilities in semiconductors with such large accumulation of acceptor units. Transient spectroscopy measurements indicate the appearance of triplet excited state species, which may be related to the semiconductors' low performances in OPVs, due to the intrusion of triplets in the carrier formation process.

1. Introduction

Organic field-effect transistors (OFETs) have been the focus of attention for many researchers in the past two decades due to their great potential as fundamental elements in electronic devices, such as, radio frequency identification (RFID) tags, smart cards,[1] electronic papers,[2] displays,[3] and sensors.[4–6] Extensive studies of OFETs have resulted in the development of organic semiconductors rivalling or surpassing the electrical performance of amorphous silicon,[7–15] and combining low-cost processability/printability with excellent mechanical flexibility.[7,16–19] However, the overall development of n-type and ambipolar semiconductors still lags behind of that of their p-type counterparts, and this is usually related to semiconductor ambient instabilities and inappropriate frontier molecular orbital alignment with electrode Fermi levels.

Ambipolar materials capable of efficiently transporting both holes and electrons by simply changing the bias voltage are extremely desirable for complementary-like electronic circuit fabrication,[19,20] and for light-emitting transistors.[21–24] For this reason, intense efforts have been devoted in recent years to the design of high-performance ambipolar small molecules and polymers. Among the most often used building blocks for ambipolar organic semiconductor design is the diketopyrrolopyrrole (DPP) core. The electron-deficient nature of DPP provides low energy LUMO levels, hence allowing the synthesis of low band-gap donor–acceptor systems when combined with thiophenic moieties (having high energy HOMOs), which have been shown to be excellent candidates for organic electronics[25–31] and photonics.[32–36] Furthermore, the possibility of ring fusion of the aromatic backbone or the tailoring of intermolecular hydrogen-bonding may yield materials with strong π–π stacking interactions and substantial orbital overlap, together with tunable HOMO and LUMO energies, which are extremely desirable features for obtaining high-performance OFETs.

In the organic electronics field, some DPP-based polymers have recently yielded ambipolar transport with mobilities

[a]Department of Organic Chemistry, Complutense University of Madrid, Faculty of Chemistry, Madrid 28040, Spain. E-mail: segura@quim.ucm.es

[b]Department of Physical Chemistry, University of Málaga, Málaga, 29071, Spain. E-mail: rocioponce@uma.es; teodomiro@uma.es

[c]Department of Chemistry and the Materials Research Center, Northwestern University, 2145 Sheridan Road, Evanston, Illinois, 60208, USA. E-mail: t-marks@northwestern.edu

† Electronic supplementary information (ESI) available: General information, synthesis and theoretical details, solar cell fabrication and characterization data. See DOI: 10.1039/c4tc00714j

surpassing 1 $cm^2\ V^{-1}\ s^{-1}$.[27,30,37–42] In comparison to DPP polymers, DPP-based small molecules have been studied to a far less extent; however, some also exhibit ambipolarity but with more modest performance, on the order of $10^{-2}\ cm^2\ V^{-1}\ s^{-1}$.[43] The inclusion of cyano functionalities in the backbone of oligothiophenes (dicyano-vinyl or tetracyanoquinodimethanes) has been successful in numerous OFET and OPV applications. Only recently, the introduction of cyano functionalities on DPP–oligothiophene cores has resulted in high-performance p-type, n-type, and ambipolar semiconductors, with hole or electron field-effect mobilities in the 0.1–1 $cm^2\ V^{-1}\ s^{-1}$ range and ambipolar mobilities of ~0.07 $cm^2\ V^{-1}\ s^{-1}$ (for holes) and 0.03 $cm^2\ V^{-1}\ s^{-1}$ (for electrons).[44–48] Inspired by these advances, we report the synthesis and properties of two new dicyanovinylene-substituted DPP–oligothiophene derivatives, **DPP-4T-2DCV** and **2DPP-6T-2DCV**, shown in Fig. 1. These two molecules possess extended π-conjugated cores and thus complement the recently published semiconductor **DPP-T-DCV** with a truncated π-core and good n-type-only thin-film mobility.[46] Importantly, the sizeable extension of the **DPP-T-DCV** π-conjugated skeleton in this work switches the transport characteristics from unipolar n-type conduction to ambipolarity.

In this contribution, we present the synthesis and characterization of two novel derivatives, **DPP-4T-2DCV** and **2DPP-6T-2DCV** (Fig. 1). The electronic and molecular structures of these two molecular semiconductors have been analyzed by electrochemistry, electronic and vibrational spectroscopy techniques, laser-flash photolysis, and quantum-chemical DFT calculations. Their electrical performances have been tested in OFET devices, showing ambipolar reasonable balanced field effect mobilities of up to 0.16–0.02 $cm^2\ V^{-1}\ s^{-1}$ for electron and hole transport, respectively.

2. Results and discussion

The synthesis of the **DPP-2T** unit was carried out as described previously.[49] Branched alkyl chains were introduced into the nitrogen centers of the **DPP-2T** monomer to increase solubility and processability from solution. Compound **2DPP-4T** was obtained by a homocoupling reaction using monobromo derivative **DPP-2T-Br** (Scheme 1). Thus, reaction of **DPP-2T** with 1.0 equiv. of NBS as the brominating agent affords a mixture of non-, mono- and dibrominated DPP derivatives that were carefully separated by flash column chromatography on silica gel. Next, the Pd-catalyzed reaction of **DPP-2T-Br** with bis-tributyltin in refluxing toluene gives dimer **2DPP-4T** that can be isolated as a dark blue solid by flash chromatography in 64% yield, together with the monostannyl derivative in 10% yield. Dimer **2DPP-4T** can also be obtained by a $PdCl_2(dppf)_2$ coupling reaction with bis-pinacolate diboron, but in lower yield (43%). Other organometallic-catalyzed coupling reactions, such as homocoupling with $Pd(OAc)_2$, oxidative coupling, CH-activation, Suzuki and Yamamoto coupling (Ni), have been recently described in analogous systems, but with the exception of the Yamamoto reaction, all dimers are obtained in lower to very poor yields.[50,51]

Bromination of dimer **2DPP-4T** with NBS in $CHCl_3$ and subsequent Stille coupling with stannyl derivative **1** affords, after hydrolysis in aqueous acid media, aldehyde **2DPP-6T-2CHO** in 62% yield. Subsequent Knoevenagel reaction with malononitrile yields **2DPP-6T-2DCV** as a dark-green solid in 70% yield (Scheme 2). Following the same methodology, bis-aldehyde **DPP-4T-2CHO** is obtained from dibromo derivative **DPP-2T-2Br** in 48% yield. Finally, compound **DPP-4T-2DCV** is obtained by reaction of **DPP-4T-2CHO** with malononitrile in moderate yield (68%; Scheme 2).

All products possess excellent solubilities and were characterized by NMR and optical spectroscopy techniques, as well as by mass spectrometry.

As expected, the ^1H NMR spectra of all derivatives are quite similar for the protons located in the aliphatic region. Thus, the first CH_2 groups of the alkyl chains attached to the N atoms of the DPP cores appear around 4.04 ppm for all compounds. A broad signal can be assigned to the C*H* proton around 1.90 ppm, and the remainder of the protons assignable to the branched alkyl chains are in the range of 1.35–0.82 ppm. Remarkably, for π-extended aldehydes **2DPP-6T-2CHO** and **DPP-4T-2CHO** the signals of the methylene protons of the *n*-hexyl substituent of the last incorporated thiophene moiety are resolved at 2.94 ppm. These protons are shielded for dicyanovinylene compounds **2DPP-6T-2DCV** and **DPP-4T-2DCV**, appearing at 2.77 and 2.76 ppm, respectively. The aromatic regions of the ^1H NMR spectra of all derivatives also exhibit common features. The comparison of the ^1H NMR spectra of

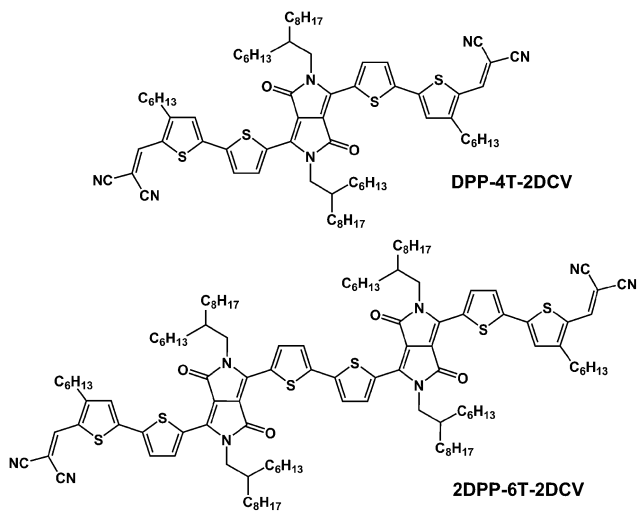

Fig. 1 Molecular structures of semiconductors DPP-4T-2DCV and 2DPP-6T-2DCV.

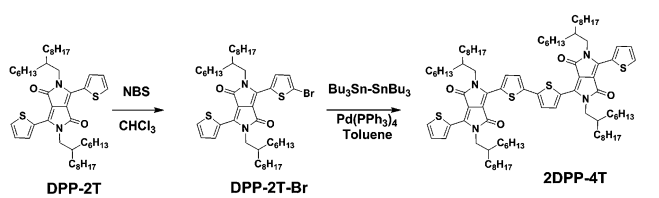

Scheme 1 Synthesis of compound 2DPP-4T.

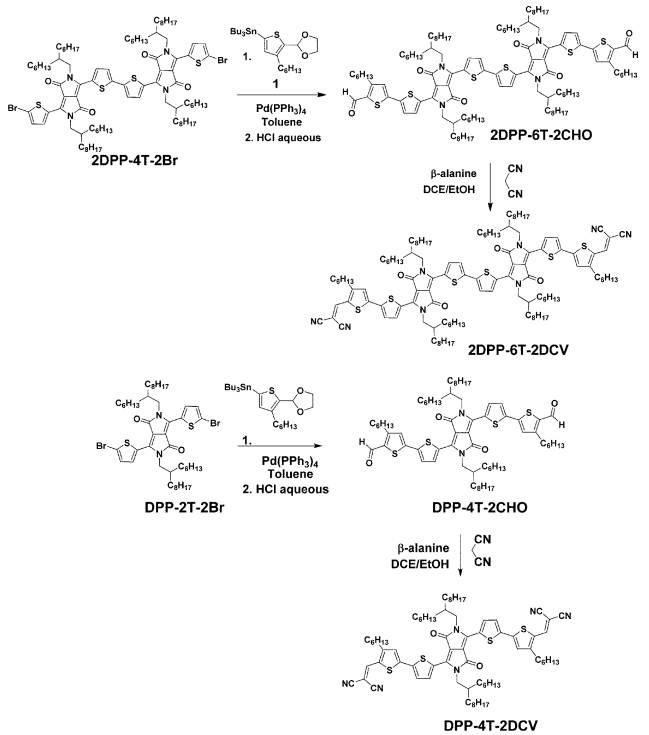

Scheme 2 Synthesis of compounds 2DPP-6T-2DCV and DPP-4T-2DCV.

dimer **2DDP-4T** and of the dibrominated derivative **2DPP-4T-2Br** allows assignment of a downfield multiplet to the overlapping signals of thiophene protons Ha and Ha* at 8.92 ppm. Ha* is shifted upfield for the dibromo derivative. The remainder of the aromatic protons can be unambiguously assigned as depicted in Fig. 2, by comparison with literature data for similar derivatives.[50,51] Significantly, aldehydes **2DPP-6T-2CHO** and **DPP-4T-2CHO** exhibit the C*H*O proton in the ^{1}H NMR spectra at 10.02 and 10.00 ppm and the olefinic protons of the terminal attached thiophene unit at 7.15 and 7.19 ppm, respectively. Finally, cyano derivatives **2DPP-6T-2DCV** and **DPP-4T-2DCV** exhibit characteristic vinyl protons at 7.82 and 7.86 ppm, respectively.

The same similarities are observed for aromatic, olefinic and aliphatic carbons in the ^{13}CNMR spectra for all derivatives. Thus, the amide group of the DPP core appears around 161 ppm and all thiophene carbons are located in the usual range. Brominated quaternary carbons in bromo derivatives **2DPP-6T-2Br** and **DPP-4T-2Br** appear upfield, as expected, at 119.0 and 119.4 ppm, respectively. Branched alkyl chains show the N–*C*H$_2$ at around 46 ppm and *C*H appears at 37 ppm in all compounds. The carbonyl moieties in bis-aldehydes **2DPP-6T-2CHO** and **DPP-4T-2CHO** appear at 181.4 and 181.6 ppm, respectively, and significantly, the vinylic carbons in tetracyano derivatives **2DPP-6T-2DCV** and **DPP-4T-2DCV** are highly shielded at 75.3 and 75.0 ppm, respectively. Finally, the IR spectra of both of these compounds clearly evidence the presence of the cyano groups at 2221 and 2222 cm^{-1}, respectively, in conjugation with the inner core.

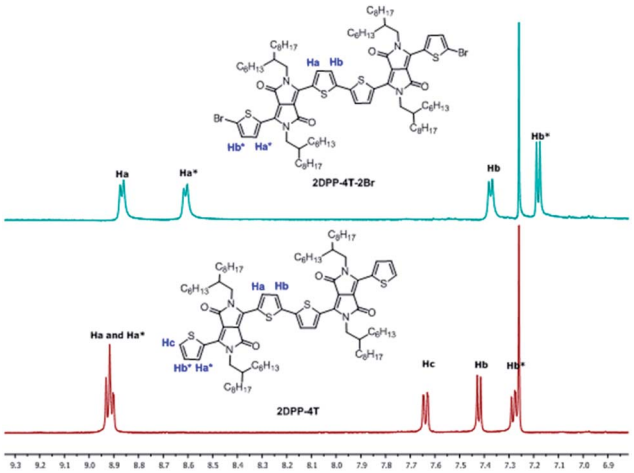

Fig. 2 Comparison of the aromatic region of the ^{1}H NMR spectra of dimer 2DDP-4T with dibrominated derivative 2DPP-4T-2Br.

2.1. Electronic structure analysis

Optical spectroscopic measurements on DPP dimer **2DPP-6T-2DCV** and its corresponding monomer **DPP-4T-2DCV** were carried out in dichloromethane solutions, showing the typical features of DPP derivatives,[52,53] with two intense bands in the 400–850 nm range (see Fig. 3).[46,54] Both systems exhibit one intense absorption peak with a λ_{max} at 730 and 642 nm, respectively. Bathochromic shifts of the absorption maxima by 88 nm are observed from **DPP-4T-2DCV** to **2DPP-6T-2DCV**. This red shift reflects the extension of the π-conjugated systems through dimerization of the DPP monomer. The optical energy gaps estimated from the onset wavelength of **DPP-4T-2DCV** and **2DPP-6T-2DCV** are 1.60 and 1.49 eV, respectively, indicating a smaller gap for the more conjugated system. Note also that the presence of the vibronic structure on the less energetic bands indicates the absence of significant intramolecular charge transfer (ICT) between the donor and acceptor parts of the molecule. This is interesting since it might reveal the possibility of a fine (step-by-step) modulation of the frontier orbital energies by a combination of donors and acceptors, an effect often impeded by ICT.

Cyclic voltammograms of **2DPP-6T-2DCV** and **DPP-4T-2DCV** were recorded in dichloromethane solutions and are shown *versus* Fc/Fc$^+$ in Fig. 4; data are compiled in Table 1. Both compounds exhibit two reversible oxidation waves. Oxidation provides a complementary view of the electronic structure of these two molecules since it takes place exclusively along the electron-rich C=C–C–C conjugated sequence, excluding the dicyanovinylene subunits.

This view is supported by quantum-chemical calculations indicating that most of the injected positive charge localizes on the thiophene rings, with a large contribution of the sulfur atoms (see ESI†). In fact, in **DPP-4T-2DCV**, each thiophene ring supports approximately 20% of the positive charge (~80% of the total), while in **2DPP-6T-2DCV** each ring supports *ca.* 15% (~90% of the total). It is interesting to emphasize that although the DPP moiety is commonly considered as an

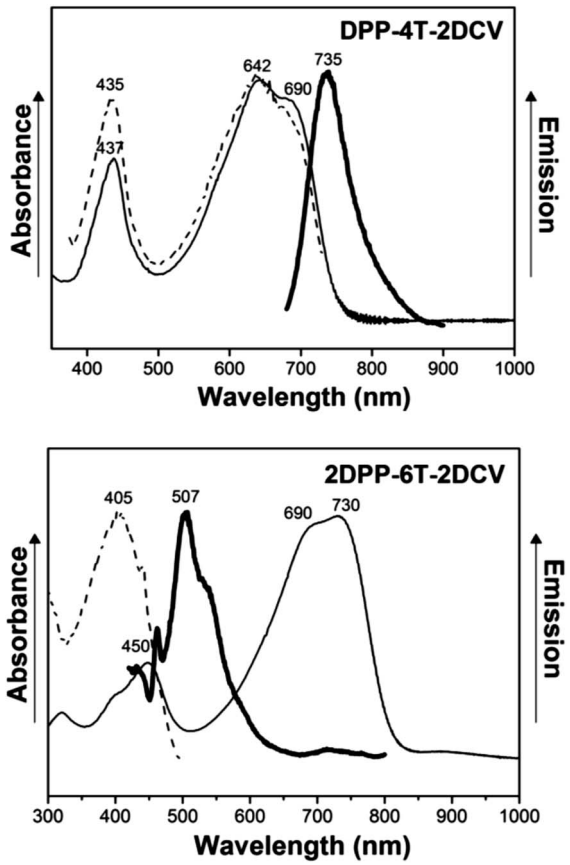

Fig. 3 Absorption (solid line), emission (bold solid line), and excitation (dashed line) spectra of the DPP-4T-2DCV and 2DPP-6T-2DCV semiconductors.

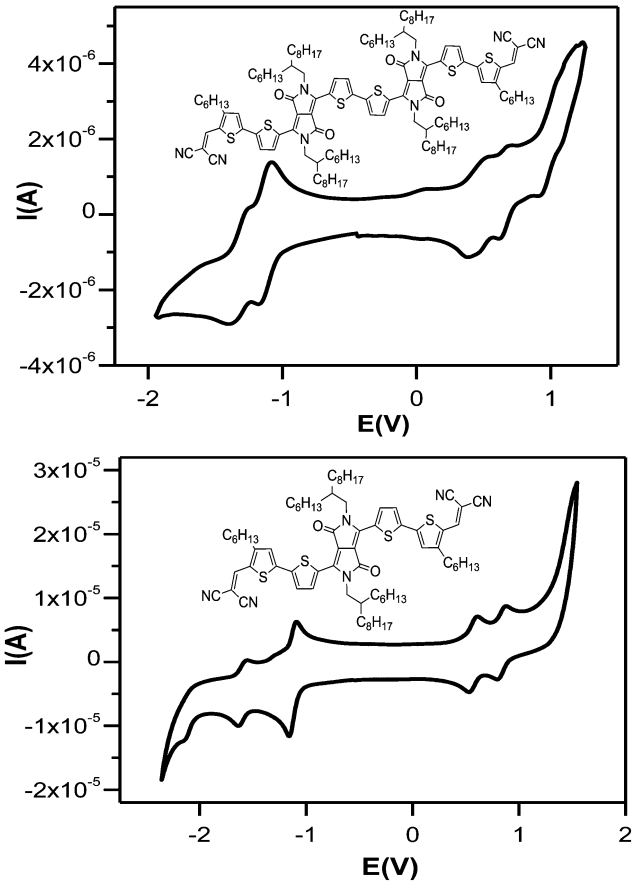

Fig. 4 Cyclic voltammograms recorded for semiconductors DPP-4T-2DCV and 2DPP-6T-2DCV in dichloromethane solution. Potentials are reference *versus* Fc/Fc^+.

electron-withdrawing group[25,32,55,56] it also bears around 20(10)% of the positive charge in **DPP-4T-2DCV(2DPP-6T-2DCV)**. This result is in good agreement with the topology of the HOMO (Fig. 5 below), where the DPP unit makes a significant contribution. This interpretation corroborates these radical cations as fully delocalized charges and therefore sensitive to the conjugation length. Thus, oxidation potentials are lower for the more extensively conjugated dimer **2DPP-6T-2DCV** in comparison with the analogous monomeric **DPP-4T-2DCV** derivative (E_{ox1} = 0.47 V, E_{ox2} 0.65 V *versus* E_{ox1} = 0.57, E_{ox2} = 0.84 V; see ESI†). In contrast to the oxidation reactions, the corresponding reductions more heavily reflect the electron-withdrawing portions of the molecules. Two reversible reduction waves are observed for both compounds: a first reduction potential at −1.12 V for **2DPP-6T-2DCV** and **DPP-4T-2DCV**, likely bielectronic processes, where charge is accumulated in the external cyanovinyl groups[57,58] (see calculated dianion charge distributions in the ESI†), and a second reductive process, associated with the DPP fragments, and logically conjugation length-dependent, −1.60 V in **DPP-4T-2DCV** and −1.32 V in **2DPP-6T-2DCV**. The result is a net lowering of the electrochemical band gap. Experimental HOMO and LUMO energies were determined from the oxidation and reduction potentials, respectively, considering that the energy level of ferrocene/ferrocenium is 4.8 eV below vacuum (see equations below), and the data obtained are summarized in Table 1.

$$E_{HOMO}: -(E_{ox} + 4.80)\ (eV)$$

$$E_{LUMO}: -(E_{red} + 4.80)\ (eV)$$

In view of the molecular orbital topologies (Fig. 5), it can be concluded for these molecules that the DPP unit heavily contributes to the HOMO; however, its contribution to the LUMO is much less pronounced.[59] This is interesting considering that the DPP building block is well-known to be electron-deficient when mixed with thiophenic fragments. In the present case, the highly electron-withdrawing dicyanovinylene groups compete with the DPP unit, greatly diminishing the acceptor character of the latter. To further analyze the contribution of the DPP unit to the HOMO, we calculated the molecular orbital (MO) energies and topologies for the **DPP-4T-2DCV** constituent units (**DCV-2T** and **DPP** units).[60] The results indicate that attaching the **DCV-2T** fragment to the **DPP** building block leaves the HOMO energy of the latter essentially unaltered, −5.45 eV (**DPP**) *versus* −5.47 eV (**DPP-2T-DCV**), indicating that the **DPP-2T-DCV** HOMO energy is dictated by the **DPP** unit and not by the

Table 1 Electrochemical potentials (V) *versus* Fc/Fc^+ of the indicated compounds in CH_2Cl_2 solution and frontier molecular orbital energies estimated from cyclic voltammetry data (DFT//B3LYP/6-31G** theoretical data are shown between brackets)

Comp.	E_{red1}	E_{red2}	E_{ox1}	E_{ox2}	E_g^{CV}	$E_g^{opt a}$	LUMO (eV)	HOMO (eV)
DPP-4T-2DCV	−1.12	−1.60	0.57	0.84	1.69	1.60	−3.68 (−3.59)	−5.37 (−5.43)
2DPP-6T-2DCV	−1.12	−1.32	0.47	0.65	1.59	1.49	−3.68 (−3.49)	−5.27 (−5.15)

[a] Optical band gap estimated from the onset of the absorption spectra.

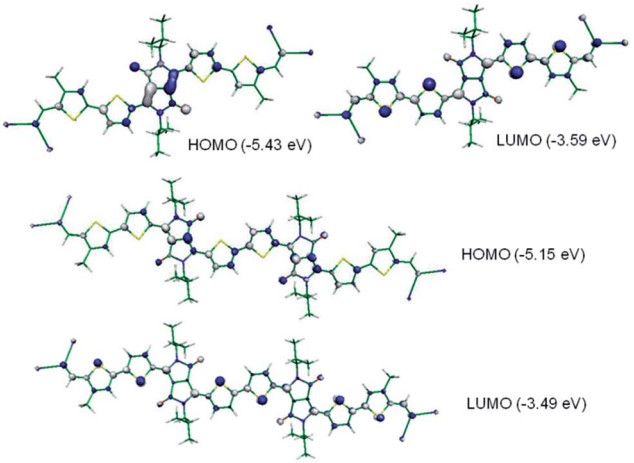

Fig. 5 B3LYP/6-31G** electronic density contours for the HOMO and the LUMO (calculated energies are shown between brackets) for **DPP-4T-2DCV** and **2DPP-6T-2DCV**.

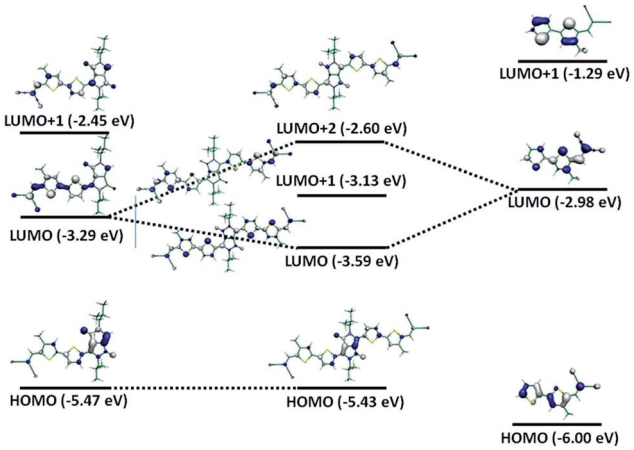

Fig. 6 B3LYP/6-31G** molecular orbital diagram showing the coupling between **DPP-2T-DCV** and the **DCV-2T** fragments.

bithiophenic fragment. The attachment of a second **DCV-2T** unit is also explored theoretically as discussed below.

Fig. 6 shows the MO diagram depicting the interaction between the **DPP-2T-DCV** and the **DCV-2T** fragments to produce **DPP-4T-2DCV**. Here we observe again that the HOMO energy is basically dictated by the HOMO of the subunit containing the DPP building block, further supporting the large contribution of that unit to the doubly-occupied orbital. Note also that in the **DPP-2T-DCV** HOMO there is a strong participation of the nitrogen atoms and the neighboring carbonyl carbon, while in the final product **DPP-4T-2DCV**, the participation of the amide nitrogen atoms is diminished in favor of the two alternate C=C double bonds of the DPP unit. Therefore, it appears that the formation of **DPP-4T-2DCV** enhances the linear conjugation between the two thiophene cores while the amide moieties remain isolated from the principal conjugated pathway, in accord with the appearance of a cross-conjugated structure competing with the primary conjugated skeleton.[61] In contrast, the LUMO orbital of **DPP-4T-2DCV** is a combination of the LUMO orbital of the constituent units, with a small contribution of the DPP unit. In fact, the wavefunction is basically localized at the molecular ends with the DPP interrupting in the middle.

2.1.1. Photophysical properties. Fig. 3 displays the absorption, excitation, and emission spectra of **DPP-4T-2DCV** and the **2DPP-6T-2DCV**. As discussed above, the absorption spectra are characterized by two principal absorptions, around 430–450 nm due to the thiophenic portion of the molecule and another, more intense band at 650–750 nm, likely involving the DPP unit together with the surrounding thiophenes. This fragmentation of the electronic structure is well corroborated by the emission spectra. In **DPP-4T-2DCV**, either by exciting the thiophene or the DPP–thiophene band, the same emission is observed from the lowest energy DPP–thiophene excited state, with a small Stokes shift. In **2DPP-6T-2DCV**, however, on exciting the thiophene part, a typical thiophene emission is observed with a characteristic vibronic structure and larger Stokes shift due to the inter-thiophene flexibility. However, by exciting the DPP–thiophene band no fluorescence is detected which is a result of the lower energy gap that accelerates the non-radiative process. Overall this is an example of emission from higher excited states (violation of the Kasha's rule) due to the energy separation between excited states imposed by the electronic structure fragmentation (cross-conjugation).

Fig. 7 displays the transient absorption spectra of **DPP-4T-2DCV** in the microsecond time regime after the excitation. The depletion of the ground electronic state absorption is clearly observed together with the emergence of a new band at 760 nm with well-defined isosbestic points, indicating the reversible transformation of the ground state molecule into a long-lived excited state, without apparent chemical degradation. For **DPP-4T-2DCV** the excited state lifetime is ~30 μs likely, indicating the presence of an absorbing triplet excited state in the flash-photolysis experiment. Residual transient absorption spectra were also observed for **2DPP-6T-2DCV**, suggesting a lower-energy photogenerated triplet state which quickly deactivates

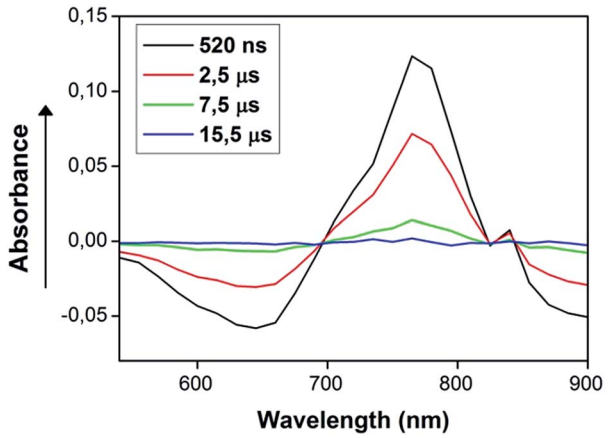

Fig. 7 Transient absorption spectra recorded for DPP-4T-2DCV in CH_2Cl_2 solution.

and eludes microsecond detection. This is in accord with the profound red-shift of the absorption spectra around 700 nm. The appearance of triplet excited state species in these molecules after laser excitation, as will be seen later, can be related to the photovoltaic activity since the formation of long-lived triplets in competition with charge transfer singlet excitons can diminish the overall yield of charge generation.

2.2. Molecular structure analysis

Fig. 8 shows the comparison between the FT-Raman spectra of **DPP-4T-2DCV** and **2DPP-6T-2DCV**. Both systems show similar spectral profiles. DFT-computed Raman spectra and selected eigenvectors for **DPP-4T-2DCV** are shown in the ESI.†

Beginning with the features at 1689 and 1688 cm^{-1} for **DPP-4T-2DCV** and **2DPP-6T-2DCV**, respectively, these are typical amide I frequencies, and thus are related to DPP-centered vibrations. To understand the implications of the energies of these vibrations we first consider two different possible vibrational couplings of the DPP unit with the surrounding core (Scheme 3). In the case of the carbonyl coupling denoted as **1** in Scheme 3, the carbonyl group is α,β linked to the neighboring vinylene fragment. Such an interaction is expected to shift the carbonyl mode to approximately 1720 cm^{-1}.[62,63] In contrast, a typical amide carbonyl group, depicted as **2** in Scheme 3, should exhibit the ν(C=O) vibration at around 1690 cm^{-1}.[63] Thus, the presence of the ν(C=O) in **DPP-4T-2DCV** and **2DPP-6T-2DCV** Raman spectra at 1689 and 1688 cm^{-1}, respectively, implies that: (i) the carbonyl vibration is more "amide-like," in line with the isolation of the carbonyl moiety from the principal linear conjugation pathway and thus, corroborates the presence of a ground state cross-conjugated structure; (ii) cross-conjugation isolates these moieties from the remainder of the conjugated skeleton and therefore, their frequencies are invariant with the molecular size. In contrast, the oligothiophene ν_{sym}(C–C/C=C) stretching vibration shifts from 1433 cm^{-1} in **DPP-4T-2DCV** to 1422 cm^{-1} in **2DPP-6T-2DCV**, in accord with elongation of the conjugational path. This vibrational scenario is consistent with the MO description discussed above, which mainly highlighted a C=C–C=C interaction through the DPP unit and consequently, more "amide-like" –N–C=O, Scheme 3 (**2**), coupling at the expense of a –C=C–C=O (**1**). The HOMO topology (Fig. 5) also reveals the electronic structure aspects of the CN group. Thus, the ν(C≡N) frequency bands are weak and frequency invariable in the **DPP-4T-2DCV** and **2DPP-6T-2DCV** Raman spectra, arguing that the wavefunction delocalization does not extend to those terminal groups and that the reduction processes, driven by the pronounced electron-withdrawing character, are confined to the dicyanovinylene groups, in agreement with the aforementioned electrochemical results. Note that the electrochemical data shown above indicate that the dicyanovinylene units were not greatly involved in the conjugational pathway, consistent with the same reduction potential for the two molecules.

2.3. Thin film properties and charge transport

Thin films of the present DPP-based semiconductors were spin-cast on OTS-treated Si/SiO_2 substrates from 10 mg mL^{-1} semiconductor solutions in chloroform, and characterized by XRD and AFM techniques. The crystallinity and long range packing

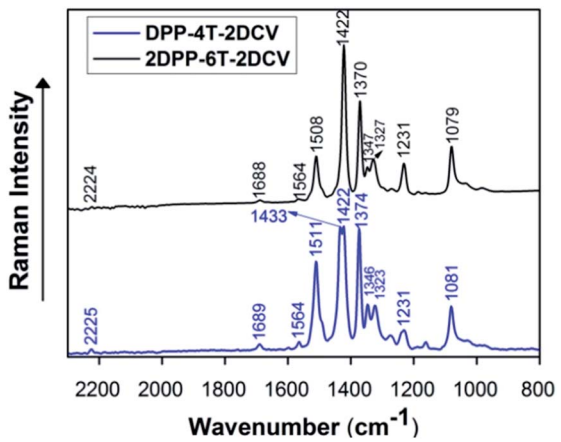

Fig. 8 FT-Raman spectra (λ_{exc}: 1064 nm) of semiconductors DPP-4T-2DCV and 2DPP-6T-2DCV in the solid state.

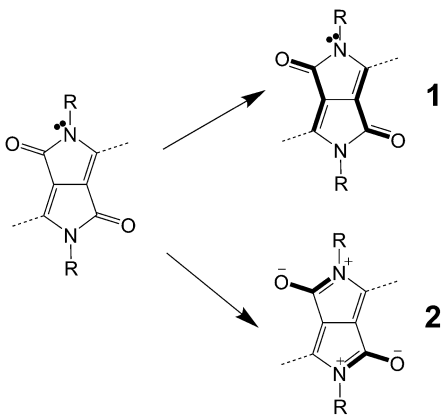

Scheme 3 Scheme indicating two different possible couplings of the DPP unit with the surrounding core.

order of **DPP-4T-2DCV** and **2DPP-6T-2DCV** thin films were studied by out-of-plane grazing incidence X-ray diffraction (GI-XRD) and data are shown in Fig. 9. The incident angle (ω) was kept low (<0.5°) to prevent the incident photons from penetrating into the substrate. Both semiconductors show modest crystalline features. The diffraction peaks at 5.0° and 4.5° correspond to lamellar packing structures with *d*-spacings of 17.6 Å and 19.6 Å for **DPP-4T-2DCV** and **2DPP-6T-2DCV**, respectively.

The occurrence of only weak second-order lamellar diffraction features in both semiconductor films suggests minimal long-range crystallinity. Note that mild annealing treatment notably enhances thin film crystallinity in both systems. In order to further explore the semiconductors' crystal structures, many attempts were made to grow single crystals but without success, which is probably due to the presence of the bulky alkyl chains in the conjugated skeletons.

The topologies of the **DPP-4T-2DCV** and **2DPP-6T-2DCV** thin films were also analyzed by tapping mode AFM. Fig. 10 shows the AFM images for as-cast films and films annealed at 80 °C. It is clear that **DPP-4T-2DCV** thin films contain much smaller grains *versus* those of **2DPP-6T-2DCV**. Although the debate is still open, larger crystalline grains are usually related to enhanced device performance. An 80 °C annealing treatment does not remarkably change the **DPP-4T-2DCV** film morphology; however in the case of **2DPP-6T-2DCV** grain connectivity is clearly diminished on mild annealing.

Solution processed bottom-gate top-contact FET devices of structure Si/SiO_x/semiconductor/Au were fabricated to assess the charge transport characteristics of **DPP-4T-2DCV** and **2DPP-6T-2DCV** films. Both semiconductors show ambipolar transport under vacuum conditions. Hole and electron mobilities were extracted in the saturated regimes from at least three separate devices from each substrate. The average and maximum field effect mobilities, along with the average threshold voltages are listed in Table 2. Some representative output and transfer plots for **DPP-4T-2DCV** and **2DPP-6T-2DCV** are shown in Fig. 11 and 12. These graphics clearly demonstrate the ambipolar nature of the charge transport characteristics.

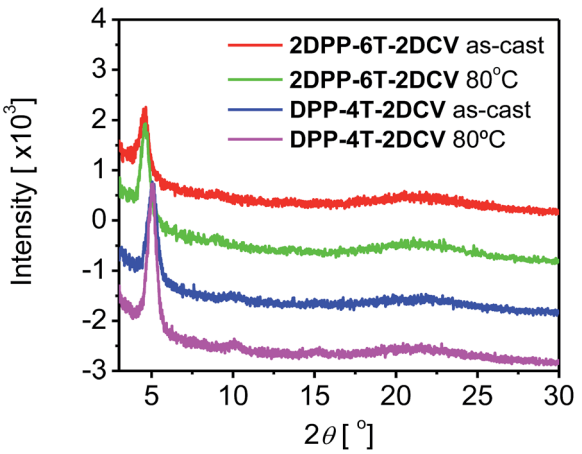

Fig. 9 Out-of-plane X-ray diffraction of as-cast and annealed (80 °C) thin films of DPP-4T-2DCV and 2DPP-6T-2DCV on OTS-modified Si/SiO_2 substrates.

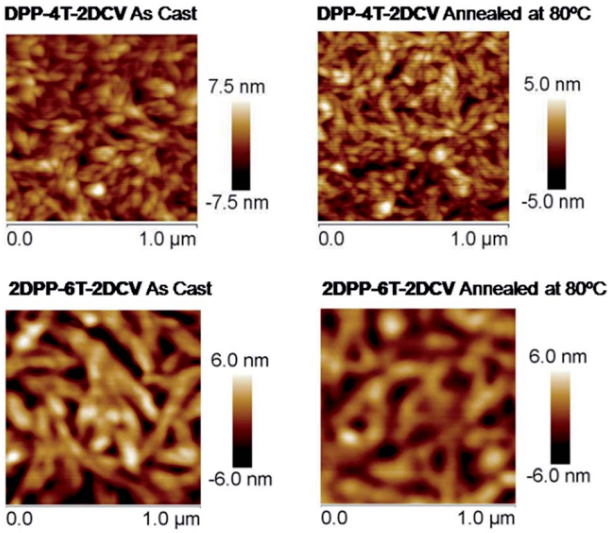

Fig. 10 Tapping-mode AFM images recorded for DPP-4T-2DCV and 2DPP-6T-2DCV under different annealing conditions.

Spin-cast films of both semiconductors exhibit excellent electron and hole transport properties under vacuum. Note that no special film casting or annealing treatment is needed to afford high performance, which is desirable for low-cost fabrication processes. The maximum electron and hole mobilities recorded for **2DPP-6T-2DCV** are 0.159 and 0.020 $cm^2\ V^{-1}\ s^{-1}$, respectively, for as-cast films. Note however that performance notably degrades on annealing. In fact, for films annealed at 80 °C substantially lower electron and hole mobilities of 0.073 and 0.013 $cm^2\ V^{-1}\ s^{-1}$ are found.

Note that these OFET data do not completely parallel the XRD/AFM microstructural trends since the XRD data show that annealed **2DPP-6T-2DCV** films are more crystalline than as-cast films, which is frequently connected with enhanced performance. However the lower OFET performance found for annealed films is indeed supported by the loss of crystallite interconnections after the thermal treatment, as shown in the AFM images.

As-cast films of **DPP-4T-2DCV** also afford sizeable electron (0.067 $cm^2\ V^{-1}\ s^{-1}$) and hole (0.008 $cm^2\ V^{-1}\ s^{-1}$) mobilities. However, in this case, the electrical performance is significantly enhanced after a mild annealing. For films annealed at 80 °C, electron and hole mobilities of 0.142 and 0.010 $cm^2\ V^{-1}\ s^{-1}$ are observed, respectively. These data are in good agreement with the previous thin film characterization, where a mild thermal annealing was translated in enhanced crystallinity without loss of intergrain connectivity.

To further understand the charge transport process we also calculated the internal reorganization energies of the neutral molecules under positive and negative charging. This theoretical parameter is related to geometrical relaxation accompanying charge transfer, and small values are desirable for efficient charge transport.[64] Intramolecular reorganization

Table 2 OFET electrical data for vapour-deposited films of the indicated semiconductors annealed under different conditions and measured in vacuum. Average field mobilities and standard deviations are shown (the highest mobility values are shown in brackets)

		n-type		p-type	
Semiconductor	Annealing temp. (°C)	μ_e ($cm^2\ V^{-1}\ s^{-1}$)	V_T (V)	μ_h ($cm^2\ V^{-1}\ s^{-1}$)	V_T (V)
DPP-4T-2DCV	As-cast	0.055 ± 0.006 (0.067)	42 ± 1	0.006 ± 0.001 (0.008)	−43 ± 1
DPP-4T-2DCV	80	0.088 ± 0.017 (0.142)	42 ± 1	0.009 ± 0.001 (0.010)	−44 ± 2
2DPP-6T-2DCV	As-cast	0.125 ± 0.009 (0.159)	41 ± 1	0.014 ± 0.002 (0.020)	−21 ± 3
2DPP-6T-2DCV	80	0.071 ± 0.001 (0.073)	22 ± 1	0.012 ± 0.001 (0.013)	−12 ± 1

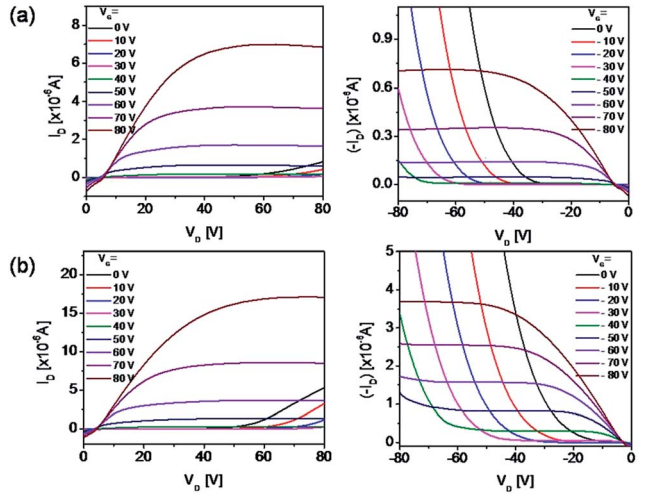

Fig. 11 Output plot data for as-cast films. (a) Left: electron transport characteristics and right: hole transport characteristics for **DPP-4T-2DCV** and (b) left: electron transport characteristics and right: hole transport characteristics for **2DPP-6T-2DCV**.

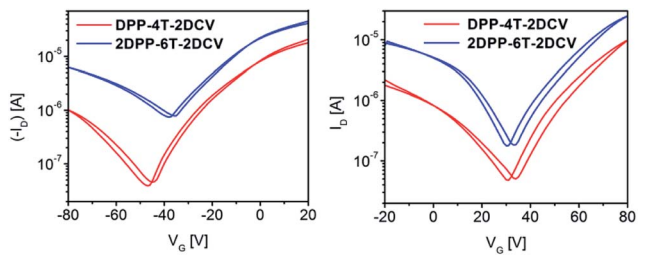

Fig. 12 Bidirectional transfer plot data for as-cast films. (a) Left: plots of **DPP-4T-2DCV** and **2DPP-6T-2DCV** under the p-type bias saturation regime ($V_D = -80$ V), (b) right: plots of **DPP-4T-2DCV** and **2DPP-6T-2DCV** under the n-type bias saturation regime ($V_D = 80$ V).

energies for electron/hole transport were estimated to be 0.21/0.22 eV and 0.16/0.18 for **DPP-4T-2DCV** and **2DPP-6T-2DCV**, respectively. The lower values found for both electron and hole transport for the molecule with the most expansive π-system is in good agreement with the higher electrical performance.

There are several examples of high hole mobility and electron mobility ambipolar materials in the literature.[40,65] Polymers containing diketopyrrolopyrrole motifs, especially when copolymerized with selenothiophene subunits, afford impressively high and balanced hole and electron mobilities in ambipolar transistors.[39,42,66–69] However, to date such high performance ambipolar characteristics have not been demonstrated in small molecules.[43,47,51,59,70–72] To the best of our knowledge, **DPP-4T-2DCV** and **2DPP-6T-2DCV** exhibit the highest balanced electron and hole mobilities in thiophene-derived small molecule ambipolar semiconductors, solution processed, or otherwise.[43,47,70,72–75] Note that the n-channel mobilities of ~0.14–0.16 $cm^2\ V^{-1}\ s^{-1}$ reported in this contribution are among the highest n-type mobilities reported to date for solution-processed small molecules.[45,70,76] Furthermore, thermal annealing is not necessary to achieve these mobility values, while in general it is needed to significantly enhance device performance.[47] This ambipolar transport behavior is nicely justified at a molecular level where the electronic structure fragmentation between donors and acceptors due to cross-conjugation imparts well differentiated molecular parts for positive and negative charge accommodation and more importantly a fine and separated tuning of the HOMO and the LUMO energy level alignment for hole and electron injection.

Further analysis of the OFET data indicates that the hole mobility is doubled in magnitude for **2DPP-6T-2DCV** *versus* **DPP-4T-2DCV** (0.02 *vs.* 0.01 $cm^2\ V^{-1}\ s^{-1}$). As noted above, the spectroscopic and quantum chemical results indicate that the positive charge is extensively delocalized over the conjugated skeleton. Therefore, a more expansive oligothiophene fragment is expected to stabilize charge injection (also facilitated by a higher HOMO energy) and transport. Note, however, that despite the more expansive **2DPP-6T-2DCV** conjugation pathway, no great differences in FET electron mobility are observed for **2DPP-6T-2DCV** *versus* **DPP-4T-2DCV**. Furthermore, it is intriguing that a semiconductor having such a large accumulation of acceptor units, up to four in the case of **2DPP-6T-2DCV**, exhibits quite balanced electron and hole mobility. We hypothesize that this is related to, among other factors, the unusual π-systems of these DPP derivatives. As shown throughout this work, the dicyanovinylene groups, the units mostly involved in the first reduction processes, are not efficiently coupled to the π-systems. In fact, despite different skeletal dimensions, both semiconductors have approximately the same LUMO energies, which, considering similar thin film characteristics, translate to similar electron mobilities (0.14 *vs.* 0.16 $cm^2\ V^{-1}\ s^{-1}$). Furthermore, the aforementioned dicyanovinylene "disconnection" with the conjugated skeleton also indicates that after electron injection, the charged defect is expected to be localized on the external parts of the molecules,

known to be a feature which leads to charge trapping in OFETs. This is the likely reason for the unexpected balanced ambipolarity in these semiconductors, and especially in **2DPP-6T-2DCV**.

2.4. Photovoltaic activity

The aforementioned promising optical, XRD, and OFET results motivated the exploration of the photovoltaic properties of the two DPP derivatives. To this end, a conventional ITO/PEDOT:PSS/semiconductor:$PC_{71}BM$/LiF/Al architecture was employed. The solar cell device performance was optimized by the variation of the active layer blend compositions and annealing temperatures. Solar cells were then fabricated with **DPP-4T-2DCV** and **2DPP-6T-2DCV** derivatives as the donor material and $PC_{71}BM$ as the acceptor (see Table 3 and ESI†). Negligible photovoltaic response is observed for **DPP-4T-2DCV**:$PC_{71}BM$ while an extremely low efficiency of 0.04% is achieved for the extended **2DPP-6T-2DCV**:$PC_{71}BM$ system. As anticipated earlier, the appearance of triplet excited state species in these molecules in the transient absorption spectroscopy could be one of the reasons behind their low performance in solar cells.[77] To further support this point, we have synthesized homologous semiconductors without the dicyanovinylene end groups, **DPP-4T** and **2DPP-6T** (Fig. 13).

While synthetic details will be reported elsewhere, it can be disclosed here that these compounds do not exhibit long-lived triplets in the transient absorption spectroscopy, and that optimized OPV structures with $PC_{61}BM$ as the acceptor yield solar cells with power conversion efficiencies of 2.36% and 0.52%, respectively (see photovoltaic characterization in the ESI†). This remarkably enhanced performance *versus* the dicyanovinylene derivatives may be related to the intrusion of triplets in the carrier formation process of the latter,[77] although it could be also partially related to different bulk heterojunction layer morphologies (see AFM images in the ESI†).

Due to the ambipolar characteristics of **DPP-4T-2DCV** and **2DPP-6T-2DCV** molecules, their ability to behave as the acceptor in the bulk heterojunction solar cells was investigated by blending them with a regioregular P3HT polymer (see data in Table 3 and ESI†). It was found that both **DPP-4T-2DCV** and **2DPP-6T-2DCV** performed better as acceptor materials than they did as donors, with a PCE of 0.08 and 0.09%, respectively. However, their performances are still remarkably low.

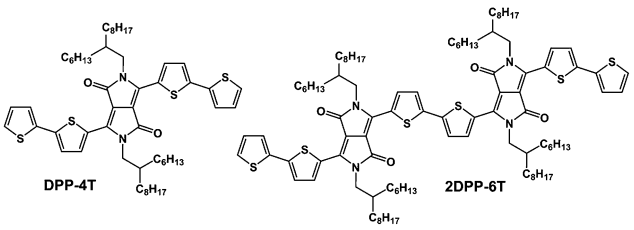

Fig. 13 Molecular structures of semiconductors DPP-4T and 2DPP-6T.

3. Conclusions

We have successfully synthesized, isolated, and characterized new *N*,*N*-alkylated DPP–thiophene conjugated derivatives. The effective synthetic pathways involve Pd-catalyzed homocoupling of the asymmetric DPP intermediate to yield the dimer **2DPP-4T**. Further functionalization of dibrominated dimer **2DPP-4T-2Br** and monomer **DPP-2T-2Br** by Stille coupling and subsequent hydrolysis and Knoevenagel reactions allow new DPP derivatives in good yields and with excellent solubilities. Optical spectra of **DPP-4T-2DCV** and **2DPP-6T-2DCV** exhibit distinctive absorptions in the 400–850 nm region, comparable to those of DPP-containing polymers. Transient absorption spectroscopy shows the presence of long-lived excited triplet states in both molecules, which may be related to their low performances found in OPVs. This could be due to charge transfer state recombination to the ground state, *via* an energetically favourable triplet state. Field-effect transistors fabricated with these semiconductors exhibit ambipolar response with balanced hole and electron mobilities, up to 0.16 $cm^2 V^{-1} s^{-1}$ and 0.02 $cm^2 V^{-1} s^{-1}$ for as-cast solution processed **2DPP-6T-2DCV** films. No thermal treatment is necessary to afford high performances, which makes this semiconductor an ideal candidate for low cost fabrication devices. Furthermore, the conjunction of electronic and vibrational spectroscopy studies, electrochemistry and DFT calculations highlights the existence of a unique electronic structure in these semiconductors, where the external cyano groups are isolated from the π-conjugated core. These unusual π-systems may account for the similar electron mobilities recorded for both **DPP-4T-2DCV** and **2DPP-6T-2DCV**, despite their different skeletal lengths. In addition, it could also be the reason behind the appearance of balanced hole and electron

Table 3 Device performance of DPP-4T-2DCV and 2DPP-6T-2DCV as both donors and acceptors in the bulk heterojunction solar cells

Donor	Acceptor	Solvent	V_{oc} [V]	J_{sc} [mA cm^{-2}]	FF [%]	PCE [%]
P3HT	**DPP-4T-2DCV**	*p*-Xylene	0.53	0.03	61	0.01
P3HT	**DPP-4T-2DCV**	*o*DCB[a]	0.53	0.24	59	0.08
P3HT	**DPP-4T-2DCV**	$CHCl_3$	0.60	0.006	51	0.002
P3HT	**2DPP-6T-2DCV**	*o*DCB	0.53	0.40	41	0.09
P3HT	**2DPP-6T-2DCV**	$CHCl_3$	0.51	0.05	39	0.01
DPP-4T-2DCV	$PC_{71}BM$	$CHCl_3$	—	—	—	—[b]
2DPP-6T-2DCV	$PC_{71}BM$	$CHCl_3$	0.48	0.25	34	0.04

[a] *o*DCB = 1,2-dichlorobenzene. [b] No photoresponse.

mobilities in semiconductors with such large accumulation of acceptor units.

Acknowledgements

We thank Comunidad Autónoma de Madrid (project S2009/MAT-1467), the UCM-BSCH joint project (GR35/10-A-910759), and the MINECO of Spain (CTQ2010-14982) for financial support of this work at Complutense University of Madrid. We also thank the AFOSR (FA9550-08-01-0331) and the NSF-MRSEC program through the Northwestern Materials Research Center (DMR-1121262) for support of this research at Northwestern University. Research at University of Malaga was supported by the MINECO (CTQ2012-33733) and Junta de Andalucia (P09-4708). R. P. O. thanks the MINECO for a "Ramón y Cajal" research contract.

Notes and references

1 D. Voss, *Nature*, 2000, **407**, 442–444.
2 J. A. Rogers, Z. Bao, K. Baldwin, A. Dodabalapur, B. Crone, V. R. Raju, V. Kuck, H. Katz, K. Amundson, J. Ewing and P. Drzaic, *Proc. Natl. Acad. Sci. U. S. A.*, 2001, **98**, 4835–4840.
3 G. Gelinck, P. Heremans, K. Nomoto and T. D. Anthopoulos, *Adv. Mater.*, 2010, **22**, 3778–3798.
4 Y. Guo, G. Yu and Y. Liu, *Adv. Mater.*, 2010, **22**, 4427–4447.
5 T. Someya, A. Dodabalapur, J. Huang, K. C. See and H. E. Katz, *Adv. Mater.*, 2010, **22**, 3799–3811.
6 P. Lin and F. Yan, *Adv. Mater.*, 2012, **24**, 34–51.
7 H. Yan, Z. H. Chen, Y. Zheng, C. Newman, J. R. Quinn, F. Dotz, M. Kastler and A. Facchetti, *Nature*, 2009, **457**, 679.
8 H. Ebata, T. Izawa, E. Miyazaki, K. Takimiya, M. Ikeda, H. Kuwabara and T. Yui, *J. Am. Chem. Soc.*, 2007, **129**, 15732–15733.
9 M. J. Kang, I. Doi, H. Mori, E. Miyazaki, K. Takimiya, M. Ikeda and H. Kuwabara, *Adv. Mater.*, 2011, **23**, 1222–1225.
10 S. W. Yun, J. H. Kim, S. Shin, H. Yang, B.-K. An, L. Yang and S. Y. Park, *Adv. Mater.*, 2012, **24**, 911–915.
11 Y. Zhao, C.-A. Di, X. Gao, Y. Hu, Y. Guo, L. Zhang, Y. Liu, J. Wang, W. Hu and D. Zhu, *Adv. Mater.*, 2011, **23**, 2448–2453.
12 Y. Mei, M. A. Loth, M. Payne, W. Zhang, J. Smith, C. S. Day, S. R. Parkin, M. Heeney, I. McCulloch, T. D. Anthopoulos, J. E. Anthony and O. D. Jurchescu, *Adv. Mater.*, 2013, **25**, 4352–4357.
13 I. Kang, H.-J. Yun, D. S. Chung, S.-K. Kwon and Y.-H. Kim, *J. Am. Chem. Soc.*, 2013, **135**, 14896–14899.
14 T. Mori, T. Nishimura, T. Yamamoto, I. Doi, E. Miyazaki, I. Osaka and K. Takimiya, *J. Am. Chem. Soc.*, 2013, **135**, 13900–13913.
15 T. Lei, J.-H. Dou, X.-Y. Cao, J.-Y. Wang and J. Pei, *J. Am. Chem. Soc.*, 2013, **135**, 12168–12171.
16 H. Sirringhaus, *Adv. Mater.*, 2005, **17**, 2411–2425.
17 S. R. Forrest, *Nature*, 2004, **428**, 911–918.
18 F. Garnier, R. Hajlaoui, A. Yassar and P. Srivastava, *Science*, 1994, **265**, 1684–1686.
19 S. Allard, M. Forster, B. Souharce, H. Thiem and U. Scherf, *Angew. Chem., Int. Ed.*, 2008, **47**, 4070–4098.
20 K.-J. Baeg, D. Khim, S.-W. Jung, M. Kang, I.-K. You, D.-Y. Kim, A. Facchetti and Y.-Y. Noh, *Adv. Mater.*, 2012, **24**, 5433–5439.
21 J. Zaumseil and H. Sirringhaus, *Chem. Rev.*, 2007, **107**, 1296–1323.
22 M. Muccini, *Nat. Mater.*, 2006, **5**, 605–613.
23 F. Dinelli, R. Capelli, M. A. Loi, M. Murgia, M. Muccini, A. Facchetti and T. J. Marks, *Adv. Mater.*, 2006, **18**, 1416–1420.
24 R. Capelli, S. Toffanin, G. Generali, H. Usta, A. Facchetti and M. Muccini, *Nat. Mater.*, 2010, **9**, 496–503.
25 Y. N. Li, S. P. Singh and P. Sonar, *Adv. Mater.*, 2010, **22**, 4862–4866.
26 T. L. Nelson, T. M. Young, J. Liu, S. P. Mishra, J. A. Belot, C. L. Balliet, A. E. Javier, T. Kowalewski and R. D. McCullough, *Adv. Mater.*, 2010, **22**, 4617–4621.
27 S. Cho, J. Lee, M. Tong, J. H. Seo and C. Yang, *Adv. Funct. Mater.*, 2011, **21**, 1910–1916.
28 H. Chen, Y. Guo, G. Yu, Y. Zhao, J. Zhang, D. Gao, H. Liu and Y. Liu, *Adv. Mater.*, 2012, **24**, 4618–4622.
29 C. Kanimozhi, N. Yaacobi-Gross, K. W. Chou, A. Amassian, T. D. Anthopoulos and S. Patil, *J. Am. Chem. Soc.*, 2012, **134**, 16532–16535.
30 J. D. Yuen, J. Fan, J. Seifter, B. Lim, R. Hufschmid, A. J. Heeger and F. Wudl, *J. Am. Chem. Soc.*, 2011, **133**, 20799–20807.
31 H. Bronstein, Z. Chen, R. S. Ashraf, W. Zhang, J. Du, J. R. Durrant, P. Shakya Tuladhar, K. Song, S. E. Watkins, Y. Geerts, M. M. Wienk, R. A. J. Janssen, T. Anthopoulos, H. Sirringhaus, M. Heeney and I. McCulloch, *J. Am. Chem. Soc.*, 2011, **133**, 3272–3275.
32 S. Loser, C. J. Bruns, H. Miyauchi, R. P. Ortiz, A. Facchetti, S. I. Stupp and T. J. Marks, *J. Am. Chem. Soc.*, 2011, **133**, 8142–8145.
33 L. Dou, J. Gao, E. Richard, J. You, C.-C. Chen, K. C. Cha, Y. He, G. Li and Y. Yang, *J. Am. Chem. Soc.*, 2012, **134**, 10071–10079.
34 S. Qu and H. Tian, *Chem. Commun.*, 2012, **48**, 3039–3051.
35 L. Dou, J. You, J. Yang, C.-C. Chen, Y. He, S. Murase, T. Moriarty, K. Emery, G. Li and Y. Yang, *Nat. Photonics*, 2012, **6**, 180–185.
36 Y. N. Li, P. Sonar, L. Murphy and W. Hong, *Energy Environ. Sci.*, 2013, **6**, 1684–1710.
37 A. R. Mohebbi, J. Yuen, J. Fan, C. Munoz, M. f. Wang, R. S. Shirazi, J. Seifter and F. Wudl, *Adv. Mater.*, 2011, **23**, 4644–4648.
38 Z. Chen, M. J. Lee, R. Shahid Ashraf, Y. Gu, S. Albert-Seifried, M. Meedom Nielsen, B. Schroeder, T. D. Anthopoulos, M. Heeney, I. McCulloch and H. Sirringhaus, *Adv. Mater.*, 2012, **24**, 647–652.
39 A. J. Kronemeijer, E. Gili, M. Shahid, J. Rivnay, A. Salleo, M. Heeney and H. Sirringhaus, *Adv. Mater.*, 2012, **24**, 1558–1565.
40 P. Sonar, S. P. Singh, Y. Li, M. S. Soh and A. Dodabalapur, *Adv. Mater.*, 2010, **22**, 5409–5413.
41 R. S. Ashraf, Z. Chen, D. S. Leem, H. Bronstein, W. Zhang, B. Schroeder, Y. Geerts, J. Smith, S. Watkins,

T. D. Anthopoulos, H. Sirringhaus, J. C. de Mello, M. Heeney and I. McCulloch, *Chem. Mater.*, 2010, **23**, 768–770.
42 J. Lee, A.-R. Han, J. Kim, Y. Kim, J. H. Oh and C. Yang, *J. Am. Chem. Soc.*, 2012, **134**, 20713–20721.
43 Y. Zhang, C. Kim, J. Lin and T.-Q. Nguyen, *Adv. Funct. Mater.*, 2012, **22**, 97–105.
44 S.-L. Suraru, U. Zschieschang, H. Klauk and F. Wurthner, *Chem. Commun.*, 2011, **47**, 1767–1769.
45 Y. Qiao, Y. Guo, C. Yu, F. Zhang, W. Xu, Y. Liu and D. Zhu, *J. Am. Chem. Soc.*, 2012, **134**, 4084–4087.
46 W. S. Yoon, S. K. Park, I. Cho, J.-A. Oh, J. H. Kim and S. Y. Park, *Adv. Funct. Mater.*, 2013, **23**, 3519–3524.
47 L. Wang, X. Zhang, H. Tian, Y. Lu, Y. Geng and F. Wang, *Chem. Commun.*, 2013, **49**, 11272–11274.
48 H. Zhong, J. Smith, S. Rossbauer, A. J. P. White, T. D. Anthopoulos and M. Heeney, *Adv. Mater.*, 2012, **24**, 3205–3211.
49 M. Castelaín, H. Salavagione and J. L. Segura, *Org. Lett.*, 2012, **14**, 2798–2801.
50 S. Stas, J.-Y. Balandier, V. Lemaur, O. Fenwick, G. Tregnago, F. Quist, F. Cacialli, J. Cornil and Y. H. Geerts, *Dyes Pigm.*, 2013, **97**, 198–208.
51 Y. Suna, J.-i. Nishida, Y. Fujisaki and Y. Yamashita, *Org. Lett.*, 2012, **14**, 3356–3359.
52 Y. Zou, D. Gendron, R. d. Badrou-Aïch, A. Najari, Y. Tao and M. Leclerc, *Macromolecules*, 2009, **42**, 2891–2894.
53 C. B. Nielsen, R. S. Ashraf, B. C. Schroeder, P. D'Angelo, S. E. Watkins, K. Song, T. D. Anthopoulos and I. McCulloch, *Chem. Commun.*, 2012, **48**, 5832–5834.
54 H. Liu, H. Jia, L. Wang, Y. Wu, C. Zhan, H. Fu and J. Yao, *Phys. Chem. Chem. Phys.*, 2012, **14**, 14262–14269.
55 Y. Li, P. Sonar, S. P. Singh, M. S. Soh, M. van Meurs and J. Tan, *J. Am. Chem. Soc.*, 2011, **133**, 2198–2204.
56 J. S. Ha, K. H. Kim and D. H. Choi, *J. Am. Chem. Soc.*, 2011, **133**, 10364–10367.
57 H. Usta, A. Facchetti and T. J. Marks, *J. Am. Chem. Soc.*, 2008, **130**, 8580–8581.
58 T. M. Pappenfus, M. W. Burand, D. E. Janzen and K. R. Mann, *Org. Lett.*, 2003, **5**, 1535–1538.
59 G. García, J. M. Granadino-Roldán, A. Hernández-Laguna, A. Garzón and M. Fernández-Gómez, *J. Chem. Theory Comput.*, 2013, **9**, 2591–2601.
60 J. Casado, M. C. Ruiz Delgado, M. C. Rey Merchán, V. Hernández, J. T. López Navarrete, T. M. Pappenfus, N. Williams, W. J. Stegner, J. C. Johnson, B. A. Edlund, D. E. Janzen, K. R. Mann, J. Orduna and B. Villacampa, *Chem.–Eur. J.*, 2006, **12**, 5458–5470.
61 R. Emanuelsson, A. Wallner, E. A. M. Ng, J. R. Smith, D. Nauroozi, S. Ott and H. Ottosson, *Angew. Chem., Int. Ed.*, 2013, **52**, 983–987.
62 H. J. Oelichmann, D. Bougeard and B. Schrader, *J. Mol. Struct.*, 1981, **77**, 179–194.
63 N. P. G. Roeges, *A Guide to the Complete Interpretation of Infrared Spectra of Organic Structures*, John Wiley & Sons Ltd., England, 1994.
64 M. Mas-Torrent and C. Rovira, *Chem. Soc. Rev.*, 2008, **37**, 827–838.
65 H. Usta, C. Newman, Z. Chen and A. Facchetti, *Adv. Mater.*, 2012, **24**, 3678–3684.
66 Y. Li, P. M. Sonar, L. Murphy and W. Hong, *Energy Environ. Sci.*, 2013, **6**, 1684–1710.
67 M. A. Naik and S. Patil, *J. Polym. Sci., Part A: Polym. Chem.*, 2013, **51**, 4241–4260.
68 J. S. Ha, K. H. Kim and D. H. Choi, *J. Am. Chem. Soc.*, 2011, **133**, 10364–10367.
69 H.-W. Lin, W.-Y. Lee and W.-C. Chen, *J. Mater. Chem.*, 2012, **22**, 2120–2128.
70 Q. Meng and W. Hu, *Phys. Chem. Chem. Phys.*, 2012, **14**, 14152–14164.
71 Y. Qiao, Y. Guo, C. Yu, F. Zhang, W. Xu, Y. Liu and D. Zhu, *J. Am. Chem. Soc.*, 2012, **134**, 4084–4087.
72 R. P. Ortiz, H. Herrera, C. Seoane, J. L. Segura, A. Facchetti and T. J. Marks, *Chem.–Eur. J.*, 2012, **18**, 532–543.
73 J. Li, X. Qiao, Y. Xiong, W. Hong, X. Gao and H. Li, *J. Mater. Chem. C*, 2013, **1**, 5128–5132.
74 J. C. Ribierre, S. Watanabe, M. Matsumoto, T. Muto, A. Nakao and T. Aoyama, *Adv. Mater.*, 2010, **22**, 4044–4048.
75 S. Handa, E. Miyazaki and K. Takimiya, *Chem. Commun.*, 2009, 3919–3921.
76 W. Hong, C. Guo, B. Sun, Z. Yan, C. Huang, Y. Hu, Y. Zheng, A. Facchetti and Y. Li, *J. Mater. Chem. C*, 2013, **1**, 5624–5627.
77 A. Rao, P. C. Y. Chow, S. Gelinas, C. W. Schlenker, C.-Z. Li, H.-L. Yip, A. K. Y. Jen, D. S. Ginger and R. H. Friend, *Nature*, 2013, **500**, 435–439.